RESEARCH ARTICLE

WILEY | HGVS HUMAN GENOME VARIATION SOCIETY

Identification and characterization of three novel mutations in the *CASQ1* gene in four patients with tubular aggregate myopathy

Virginia Barone[1]* | Valeria Del Re[1]* | Alessandra Gamberucci[1] | Valentina Polverino[1] |
Lucia Galli[2] | Daniela Rossi[1,2] | Elisa Costanzi[3] | Luana Toniolo[4,5] | Gianna Berti[6] |
Alessandro Malandrini[6] | Giulia Ricci[7] | Gabriele Siciliano[7] | Gaetano Vattemi[8] |
Giuliano Tomelleri[8] | Enrico Pierantozzi[1] | Simone Spinozzi[1] | Nila Volpi[6] |
Rosella Fulceri[1] | Roberto Battistutta[3] | Carlo Reggiani[4,5] | Vincenzo Sorrentino[1,2] iD

[1]Department of Molecular and Developmental Medicine, Molecular Medicine Section, University of Siena, Siena, Italy

[2]Azienda Ospedaliera Universitaria Senese, Siena, Italy

[3]Department of Chemical Sciences, University of Padova, Padova, Italy

[4]Department of Biomedical Sciences, University of Padova, Padova, Italy

[5]CNR, Institute of Neuroscience, Padova, Italy

[6]Department of Medical, Surgical and Neurological Sciences, University of Siena, Siena, Italy

[7]Department of Clinical and Experimental Medicine, University of Pisa, Pisa, Italy

[8]Department of Neurological Neurosciences, Biomedicine and Movement Sciences, Section of Clinical Neurology, University of Verona, Verona, Italy

Correspondence
Vincenzo Sorrentino, Molecular Medicine Section, Department of Molecular and Developmental Medicine, University of Siena, Siena, Italy.
Email: vincenzo.sorrentino@unisi.it

*Virginia Barone and Valeria Del Re contributed equally to this work.

Communicated by Johan T. den Dunnen

Abstract

Here, we report the identification of three novel missense mutations in the calsequestrin-1 (*CASQ1*) gene in four patients with tubular aggregate myopathy. These CASQ1 mutations affect conserved amino acids in position 44 (p.(Asp44Asn)), 103 (p.(Gly103Asp)), and 385 (p.(Ile385Thr)). Functional studies, based on turbidity and dynamic light scattering measurements at increasing Ca^{2+} concentrations, showed a reduced Ca^{2+}-dependent aggregation for the CASQ1 protein containing p.Asp44Asn and p.Gly103Asp mutations and a slight increase in Ca^{2+}-dependent aggregation for the p.Ile385Thr. Accordingly, limited trypsin proteolysis assay showed that p.Asp44Asn and p.Gly103Asp were more susceptible to trypsin cleavage in the presence of Ca^{2+} in comparison with WT and p.Ile385Thr. Analysis of single muscle fibers of a patient carrying the p.Gly103Asp mutation showed a significant reduction in response to caffeine stimulation, compared with normal control fibers. Expression of CASQ1 mutations in eukaryotic cells revealed a reduced ability of all these CASQ1 mutants to store Ca^{2+} and a reduced inhibitory effect of p.Ile385Thr and p.Asp44Asn on store operated Ca^{2+} entry. These results widen the spectrum of skeletal muscle diseases associated with *CASQ1* and indicate that these mutations affect properties critical for correct Ca^{2+} handling in skeletal muscle fibers.

KEYWORDS
calsequestrin, excitation–contraction coupling, ORAI1, SOCE, STIM1, tubular aggregate myopathy

1 | INTRODUCTION

Calsequestrin (CASQ) is a protein of 45 kDa localized in the lumen of the sarcoplasmic reticulum (SR) of striated muscles where, thanks to its ability to bind Ca^{2+} with low affinity and high capacity, is responsible for Ca^{2+} storage in relationship with activation of muscle contraction. Two isoforms of CASQ, encoded by two different genes, have been identified: the skeletal isoform CASQ1 (MIM# 114250) expressed in fast skeletal muscle fibers and the cardiac isoform CASQ2 (MIM# 114251) expressed in cardiac muscle and slow skeletal muscle fibers (Schiaffino & Reggiani, 2011). Mutations in the *CASQ2* gene have been associated to catecholaminergic polymorphic ventricular tachycardia (Lahat et al., 2001). This disorder is usually caused by emotional stress or exercise in young individuals, and is characterized by recurrent syncopal episodes and seizures or sudden death due to the impaired Ca^{2+} handling properties of cardiomyocytes expressing mutated CASQ2 (Faggioni, Kryshtal, & Knollmann, 2012). More recently, we reported the first mutation in *CASQ1* in patients with vacuolar aggregate myopathy (MIM# 616231), an autosomal dominant muscle disorder characterized by the presence of large vacuoles containing distinctive inclusions of variable size that result from the aggregation of SR proteins (Rossi et al., 2014b; Tomelleri et al., 2006).

In the SR of skeletal muscle fibers, CASQ1 may exist both as monomers and polymers, where polymerization depends on Ca^{2+} concentrations. Low concentrations of Ca^{2+} induce dimerization by favoring front-to-front interactions between two adjacent monomers. Further increases in Ca^{2+} levels lead to the formation of polymers, mediated by back-to-back interactions, that result in an increased ability to bind Ca^{2+} (Park, Wu, Dunker, & Kang, 2003; Sanchez et al., 2012). CASQ1 participates, together with other proteins as triadin, junctin, and the ryanodine receptor Ca^{2+} release channel (RyR1) in the assembly of a large macromolecular machinery dedicated to Ca^{2+} release from the SR (Barone, Randazzo, Del Re, Sorrentino, & Rossi, 2015). Previous studies have provided evidence that CASQ1 may have an inhibitory effect on the pathways that regulate Ca^{2+} entry (Shin et al., 2003; Zhao et al., 2010). A physical interaction between CASQ1 and the Stromal Interaction Molecule 1 (STIM1), localized on the SR, has been also reported (Wang et al., 2015; Zhang, Wang, Li, Xue, & Luo, 2016). STIM1, together with the Ca^{2+} release-activated Ca^{2+} modulator 1 (ORAI1) on the plasma membrane, functions to allow the replenishing of depleted intracellular Ca^{2+} stores, a mechanism known as Store-Operated Ca^{2+} Entry (SOCE).

Recently, missense mutations in *STIM1* (MIM# 605921) and *ORAI1* (MIM# 610277) genes have been identified in patients affected by tubular aggregate myopathy (TAM) (Böhm et al., 2013, 2014, 2017; Endo et al., 2015; Okuma et al., 2016). TAM is a progressive condition characterized by muscle weakness, cramps, myalgia, and the presence of tubular aggregates in muscle fibers that originate from the SR membrane (Engel, Bishop, & Cunningham, 1970) and contain numerous SR proteins including, among others, sarco-endoplasmic reticulum Ca^{2+} ATPase (SERCA), triadin, and CASQ1 (Chevessier et al., 2005; Salviati et al., 1985; Boncompagni, Protasi, & Franzini-Armstrong, 2012). The processes leading to the formation of these structures are not fully understood. Tubular aggregates formation has been proposed to result

from aggregation of SR-derived membranes possibly caused by misfolding and aggregation of SR proteins as a consequence of hereditary or acquired conditions (Agbulut, Destombes, Thiesson, & Butler-Browne, 2000; Chevessier et al., 2005; Giacomello et al., 2015; Kuncl, Pestronk, Lane, & Alexander, 1989; Schiaffino, 2012). Activating mutations in *STIM1* have been also detected in patients with Stormorken syndrome, who present thrombocytopenia and bleeding diathesis in association with miosis and TAM (Misceo et al., 2014; Nesin et al., 2014). Activating mutations in *ORAI1* have been detected in patients with a Stormorken-like syndrome lacking hematological disorders but presenting with miosis and TAM (Nesin et al., 2014). On the other hand, loss-of-function mutations in *ORAI1* and *STIM1* have been detected in patients with severe combined immunodeficiency syndrome that also present a non-progressive muscle hypotonia (Feske et al., 2006; Maus et al., 2015) indicating that mutations resulting in either decreased or increased Ca^{2+} influx have the potential to affect skeletal muscle tissue (Lacruz & Feske, 2015).

Here, we report the first identification of three different mutations in the *CASQ1* gene in patients with TAM. Characterization of these CASQ1 mutations indicated that they have altered Ca^{2+}-dependent polymerization and reduced ability to store Ca^{2+}.

2 | MATERIALS AND METHODS

2.1 | Ethics statement

Ethics committee approval and written informed consent was obtained for all patients. This study complies with the ethical standards laid down in the 1964 Declaration of Helsinki.

2.2 | Morphological analysis of patients' muscle biopsies

All patients underwent an open biopsy of vastus lateralis muscle. Serial 10 μm-thick transversal or longitudinal sections were stained with standard histological and histochemical methods including hematoxylin and eosin (H&E), reduced nicotinamide adenine dinucleotide-tetrazolium reductase (NADH), succinate dehydrogenase (SDH), and cytochrome *c* oxidase (COX). For immunofluorescence experiments, 8 μm-thick sections were incubated with the following primary antibodies: anti-CASQ1 mouse monoclonal antibody (clone MA3-913; ThermoFisher Scientific, Waltham, MA); anti-CASQ1 rabbit polyclonal antibody (ThermoFisher Scientific, Waltham, MA); anti-STIM1 mouse monoclonal antibody (clone 44/GOK; BD Biosciences, Franklin Lakes, New Jersey), anti-ORAI1 mouse monoclonal antibody (clone 6D11A11; ThermoFisher Scientific, Waltham, MA), anti-SERCA mouse monoclonal antibody (clone IIH11; ThermoFisher Scientific, Waltham, MA), and anti-RyR1 rabbit polyclonal antibody (Rossi et al., 2014a). Cy2- or Cy3-conjugated antimouse or antirabbit secondary antibodies (Jackson ImmunoResearch Laboratories, Westgrove, PA) were used for immunofluorescence detection. All procedures for histochemical and electron microscope analysis have been previously described (Rossi et al., 2014b; Tomelleri et al., 2006).

2.3 | Genetic analysis

Genomic DNA was extracted from peripheral blood leucocytes by standard procedures. All *CASQ1* exons were amplified using specific primers designed with Primer3 software (https://bioinfo.ut.ee/primer3). Amplified DNA fragments were directly sequenced using an ABI Prism 310 apparatus (Applied Biosystems, Waltham, MA) as previously described (Rossi et al., 2014b). DNA mutation numbering was based on cDNA reference sequence (NM_001231.4), taking nucleotide +1 as the A of the ATG translation initiation codon. The mutation nomenclature used follows that described at https://www.hgvs.org./mutnomen/. The CASQ1 mutations have been submitted to the locus-specific database (www.lovd.nl/CASQ1).

Whole-exome sequencing (WES) was performed at CRIBI Biotechnology Center (Padova, Italy). Briefly, DNA libraries were constructed following the standard protocol of the Ion AmpliSeq™ Exome RDY Kit (ThermoFisher Scientific, Waltham, MA). Starting from 100 ng of gDNA, a multiplex-PCR with 12 primer pools was perfomed, allowing the amplification of 24,000 amplicons per pool, covering the exonic regions of the genomes (about 58 Mb). Further, 9 μl of 100 pM barcoded libraries were amplified by emulsion PCR in the OneTouch2 instrument.

Finally, the barcoded samples were loaded into Ion Proton P1 v3 chip and sequenced on the Ion Proton instrument using the Ion Proton HiQ Sequencing kit. The bioinformatic analysis was performed on the Ion Torrent Server and the Torrent SuiteTM (https://ts-pgm.epigenetic.ru/ion-docs/Torrent-Variant-Caller-Plugin.html) for variant calling and to align the reads to the human genome reference 19 (hg19, https://grch37.ensembl.org/). Data were then analyzed by QueryOR web platform (https://queryor.cribi.unipd.it/cgi-bin/queryor/mainpage.pl) (Bertoldi et al., 2017) and genetic variants (missense, nonsense, indels) filtered for a global minor allele frequency ≤0.001, shared by the affected individuals but not present in five healthy controls. Multiple protein alignment was performed using the ClustalW software (https://www.ebi.ac.uk/Tools/msa/clustalo/). Structural analysis of CASQ1 mutations was performed using the "PyMOL molecular visualization system" (https://pymol.org) on the crystal structure of hCASQ1 (PDB code: 3UOM).

2.4 | Generation and purification of recombinant CASQ1

The human CASQ1 cDNA (NM_001231.4) was amplified by polymerase chain reaction (PCR) using specific primers with *Bam*HI and *Sal*I restriction sites (Forward: 5′ cgg gat cca tgg ggc cca gag ctg tgc cg; Reverse: 5′ gac gtc gac cta gtc atc atc atc atc gtc). The cDNA was cloned in frame with GST in the plasmid vector pGEX-4T-1 (GE Healthcare, Chicago, Illinois) digested with the same restriction enzymes. Site-directed mutagenesis of double-stranded cDNA was performed using the Q5 Site-Directed Mutagenesis Kit (NEB Inc, Ipswich, MA). All the constructs were sequenced using an ABI Prism 310 apparatus (Applied Biosystems, Waltham, MA). Recombinant plasmids were transformed by electroporation in the BL21 *E. coli* strain. Expression and purification of recombinant proteins have been previously described (Rossi et al., 2014a). Thrombin cleavage was performed to separate GST from the protein of interest using the Thrombin Cleavage Capture Kit (Millipore) according to manufacturer's instructions.

2.5 | Limited trypsin proteolysis assay

Wild-type (WT) and mutant CASQ1 proteins were incubated in 20 mM Tris–HCl, pH 7.4 at 25°C for 20 min in a reaction volume of 100 μl in the presence or absence of 0, 1, 3 mM Ca^{2+}. Five micrograms of protein was taken before trypsin (Sigma-Aldrich, St. Louis, Missouri) was added at a protease:CASQ1 ratio of 1:500 (w/w). Samples (5 μg) were taken at specific time points of 5, 30, and 120 min, mixed with sample buffer 4× to stop trypsin proteolysis and heated at 95°C for 3 min before the analysis on 15% SDS-PAGE. The gels were stained with Blue-Coomassie. Experiments were repeated at least three times.

2.6 | Turbidity assay, dynamic light scattering, and structural analysis

Turbidity assay was performed to study CASQ1 aggregation as a function of Ca^{2+} concentration (Scherer, Leung, Owyang, & Shire, 2012). Turbidity was detected using a spectrophotometer and measuring the absorbance at 350 nm. In particular, 2.5 μM of protein was incubated in 100 μl of a solution containing 20 mM Tris–HCl and 150 mM KCl, pH 7.4 in a quartz micro cuvette. Increasing Ca^{2+} concentrations from 0 to 10 mM were added in the sample and mixed by pipetting. Absorbance measurements were recorded at intervals of 10 min at 25°C. Experiments were repeated at least three times. The Ca^{2+}-dependent aggregation of the proteins was analyzed also by dynamic light scattering (DLS), using a Zetasizer Nano˙ (Malvern Instruments, Malvern, U.K.) and a low volume quartz cuvette. Samples were centrifuged at 10,000 g for 10 min and filtered using 0.45 μm filters prior to data collections. Measurements were performed at 25°C with 3 mg/ml of protein buffered in 20 mM Tris–HCl, 300 mM KCl, pH 7.4, with the following Ca^{2+} concentrations: 0, 3, 5, and 10 mM. To evaluate the reversibility of the aggregation process, 10 mM EGTA was added at the sample with 10 mM Ca^{2+}.

2.7 | Patient's single fiber Ca^{2+} release and force measurement

Small fragments of muscle biopsies were immersed in glycerol-containing skinning solution (Salviati & Volpe, 1988). Single fibers were manually dissected and segments of approximately 1-mm in length were cut and mounted with small aluminum clips (T clips) at both ends. The experimental setup has been previously described (Doria et al., 2011). The ability of the SR to store and release Ca^{2+} was tested with a protocol of cyclic SR loading in the presence of ATP at low pCa^{2+} and releasing Ca^{2+} with caffeine in low Mg^{2+} and low EGTA (Rossi et al., 2014b, Rossi, Bottinelli, Sorrentino, & Reggiani, 2001). Caffeine concentrations tested were in the range 0.5–20 mM, the latter being sufficient to induce a maximal release, virtually emptying SR (Fryer & Stephenson, 1996; Lamb, Cellini, & Stephenson, 2001; Lamboley et al., 2015). Therefore, maximal response to caffeine provided an approximation of the total Ca^{2+} content of the SR, while the curve linking the

amount of Ca^{2+} release to the caffeine concentration was taken as an indication of the ryanodine receptor channel properties. Tension time area, normalized to the amplitude of the contractile response elicited by a direct maximal activation with pCa 4.3, was adopted as an indication of the amount of Ca^{2+} released (Endo & Iino, 1988; Lamboley et al., 2015; Makabe, Werner, & Fink, 1996, Fryer & Stephenson, 1996, Lamb et al., 2001).

2.8 | Cell culture, DNA transfection, and Ca^{2+} measurement

HeLa cells were cultured in DMEM supplemented with 10% heat-inactivated fetal bovine serum as previously described (Giurisato et al., 2014). Cells were plated on four-wells glass chambers slides (Sarstedt, Nümbrecht, Germany) at the density of 4×10^4 cells/chamber. After 24 hr, cells were co-transfected with pcDNA3.1 vectors expressing CASQ1 and GFP using Lipofectamine-Plus reagent following the manufacturer's instructions. Changes in cytosolic Ca^{2+} concentration were measured with Fura-2/AM (Life Technologies, Waltham, MA). Transfected HeLa cells were loaded with 3 μM Fura-2 as described (Giurisato et al., 2014). Transfected cells were identified by detection of GFP fluorescence and only cells expressing comparable levels of GFP fluorescence were selected. For Ca^{2+} measurements, Fura-2 fluorescence was analyzed with a MetaFluor imaging system; experiments were carried out at room temperature in Ca_{2+}-free solution containing 0.5 mM EGTA. Ca^{2+} release from the endoplasmic reticulum (ER) was induced by 1μM Thapsigargin (Tg; Sigma-Aldrich, St. Louis, Missouri). Ca^{2+} influx was evaluated following the addition of 1.5 mM $CaCl_2$. The ratio (R) between fluorescence signals 340/380 nm was used to calculate cytosolic Ca^{2+} concentration according to the following formula: $[Ca^{2+}]_i = K_d * [(R - R_{min})/(R_{max} - R)] * Sf/Sb$; R_{max} was obtained by treating the cells with 5 μM ionomycin and 10 mM Ca^{2+} and R_{min} by adding 5 μM ionomycin and 20 mM EGTA in Ca^{2+}-free Hepes buffer. Sf and Sb are the emission intensities at 380 nm for Ca^{2+} free and Ca^{2+} bound Fura-2, respectively. K_d for Fura-2 at 25°C was assumed 135 nM. In order to quantify the Ca^{2+} released from the ER, the area under the curve (AUC), which represents the Ca^{2+} released in 5 min after the addition of Tg, was measured. An indication of Ca^{2+} influx was calculated measuring the difference between $[Ca^{2+}]_i$ peak after Ca^{2+} re-addition and basal $[Ca^{2+}]_i$. Statistical significance was estimated by the two-tailed unpaired Student's test with systematic Welch correction for variance with GraphPad Prism 6.0.

2.9 | Time-lapse live imaging and image analysis

GFP-fusion proteins were obtained by cloning WT and mutant CASQ1 cDNAs in the pEGFP expression vector (Clontech Laboratories, Mountain View, CA). HeLa cells were co-transfected with vectors expressing WT or mutant GFP-CASQ1 and mRFP-STIM1 (Giurisato et al., 2014). Cells were plated on four-chamber glass bottom dishes (In vitro Scientific, Mountain View, CA) and treated with 1 μM Tg to induce SOCE in Hepes buffer medium. Time-lapse live imaging was performed with a confocal laser scan microscopy (Zeiss LSM 510 Meta). Single cells were selected and top to bottom focal planes were acquired at a time

interval of 3 min, at a 1024×1024 resolution and with a maximum voxel size of $0.11 \times 0.11 \times 1$ μm (X, Y, and Z dimensions). The distribution of the CASQ1 GFP fluorescence signal was evaluated by counting the number of cells showing linear structures, round structures and a homogeneous distribution in the ER at $t = 0$ and $t = 12$ min after Tg addition. The relative percentage of each class of distribution was calculated and expressed as average value from at least four independent experiments. Statistical analysis was performed with GraphPad Prism 6.0 software and the Holm-Sidak's multiple comparisons test. Image analysis was performed with ImageJ software v.10.2 (https://imagej.nih.gov/ij/). For evaluation of the average size of mRFP-STIM1 clusters, selected images were corrected for background fluorescence. The ImageJ "Auto Threshold" function (version 1.14) of the GDSC plugin was set on corrected images and average size of clusters was calculated using the ImageJ "Analyze Particles" plugin. Statistical analysis was performed with GraphPad Prism 6.0 software and the Holm-Sidak's multiple comparisons test.

3 | RESULTS

3.1 | Missense variants in the *CASQ1* gene are present in four patients affected by TAM

Sequence analysis of the *CASQ1* gene (NC_000001.11) in a group of 21 patients with a clinical history of molecularly undiagnosed myopathy resulted in the identification of a NM_001231.4:c.130G > A variant, predicting an amino acid change from aspartic acid to asparagine (p.(Asp44Asn), RNA not analyzed), in a 32-year-old male (patient 1), who complained of fatigue and diffuse exercise-induced myalgia. Electromyography showed a myopathic pattern in the muscles examined (bilateral anterior tibial, rectus femoris, deltoid and biceps brachii, and right vastus median). Repetitive stimulation excluded neuromuscular junction disorders. Echocardiography and electrocardiogram were normal. At the histological level, patient 1 presented features of tubular aggregates compatible with a diagnosis of TAM (Figure 1A). Based on this evidence, we extended the analysis to seven unrelated patients with a diagnosis of TAM. This analysis resulted in the identification of two additional *CASQ1* heterozygous missense variants in three patients (Figure 1B). The NM_001231.4:c.308G > A variant, predicting an amino acid change from glycine to aspartic acid (p.(Gly103Asp), RNA not analyzed), was found in two different probands, a 67-year-old male (patient 2) who complained of fatigue, and a 52-year-old woman (patient 3) with a 10-year history of exercise-induced muscle pain, stiffness, and early fatigue. The NM_001231.4:c.1154T > C variant, predicting an amino acid change from isoleucine to threonine (p.(Ile385Thr) RNA not analyzed), was detected in an 82-year-old woman (patient 4) suffering of myalgia and proximal muscle weakness (Figure 1B). The serum CK was normal in all patients except for patient 2, who exhibited occasional elevation of CK serum (752 UI/l). No family history has been documented for these patients.

Light microscopy analysis of muscle biopsies of all probands revealed, as a distinguishing feature, the presence of tubular aggregates mainly in type II fibers that stained strongly with NADH, whereas
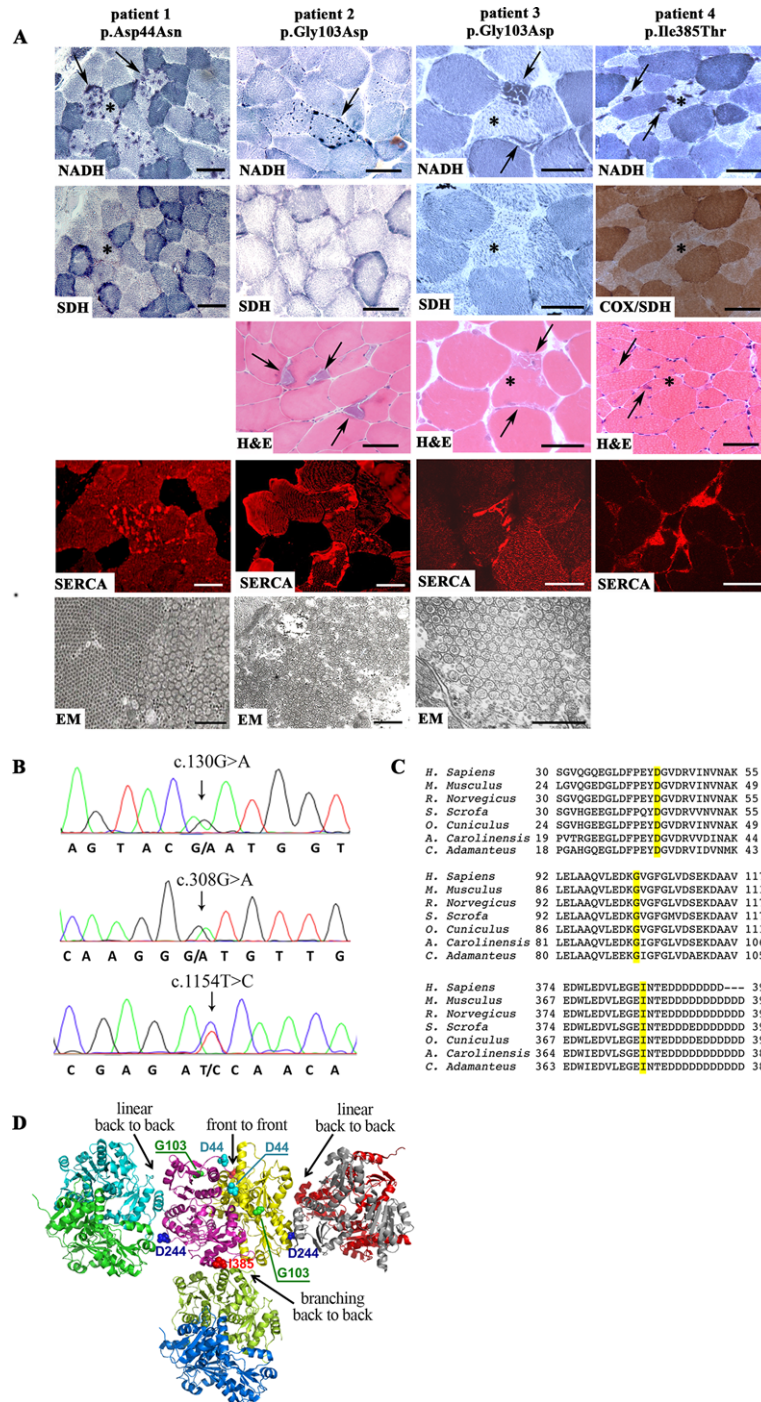
FIGURE 1 Histological, immunohistochemical, and ultrastructural characterization of patients' muscle biopsies. **A**: Tubular aggregates were basophilic following hematoxylin and eosin (H&E). Tubular aggregates stained in dark blue by nicotinamide adenine dinucleotide-tetrazolium reductase reaction (NADH), whereas they were not detected by either succinate dehydrogenase (SDH) or cytochrome c oxidase (COX) staining. Arrows point to tubular aggregates. Asterisks denote the same fiber in serial biopsy sections. All patients' biopsies displayed tubular aggregates that were stained by anti-SERCA1 antibody. Electron microscopy (EM) analysis confirmed the presence of tubular aggregates. EM micrographs were not available for patient 4. Bars: 50 μm in H&E, NADH, COX, and SERCA1 pictures; 1 μm in EM micrographs. **B**: Electropherogram of the *CASQ1* gene sequence of patients heterozygous for the c.130G > A (patient 1), c.308G > A (patients 2 and 3) and c.1154T > C (patient 4). **C**: Protein sequence alignment of CASQ1 regions of different species: the aspartic acid (D) in position 44, the glycine (G) in position 103 and the isoleucine (I) in position 385 are highlighted in yellow and are conserved among species ranging from snakes to humans. **D**: Proposed model of polymerization based on the crystal structure of CASQ1 in presence of high Ca^{2+} (PDB-ID 3UOM). Dimers of CASQ1 held together by front-to-front interactions (yellow and magenta monomers) can interact with other dimers both via "linear" back-to-back contacts (dimers green/cyan and red/gray) and via "branching" back-to-back contacts (dimer blue/olive green), originating a branched polymer. Mutation in position 244 (blue spheres for Asp244) interferes with linear back-to-back contacts while mutation in position 385 interferes (red spheres for Ile385) with branching back-to-back contacts. Residues Asp44 and Gly103 are indicated by light blue and green spheres, respectively, and both are localized at the front-to-front interaction surface where they can interfere with dimer formation
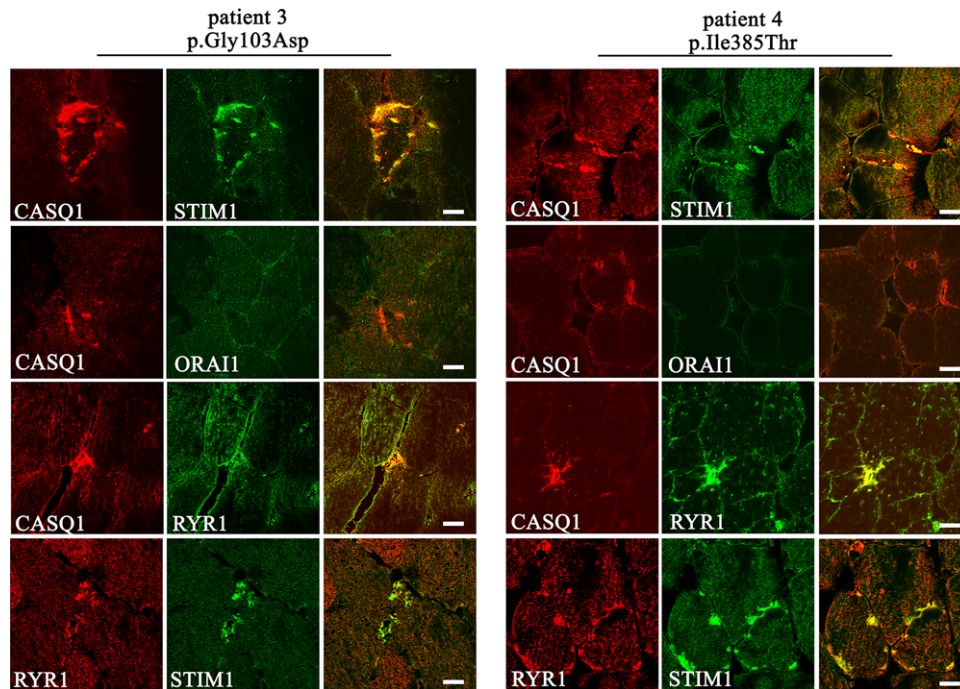
FIGURE 2 Immunofluorescence experiments on cross sections of biopsies from patients 3 and 4 revealed that nearly all tubular aggregates contained CASQ1. The vast majority of CASQ1 positive tubular aggregates were also positive for STIM1 and RYR1, whereas ORAI1 was rarely detected and at much lower extent in CASQ1 positive aggregates. Bars: 20 μm

they were negative to SDH or COX staining, indicating a reticular rather than a mitochondrial origin of the aggregates (Figure 1A). Biopsies of patients 2, 3, and 4 were also stained with H&E, which stains tubular aggregates in pink. Electron microscopy analysis was performed on specimens from patients 1, 2, and 3 and showed the typical presence of cytoplasmic aggregates of swollen membranous tubules. Immunostaing of cross sections from all patients' biopsies with antibody against SERCA confirmed the SR origin of these aggregates (Figure 1A). Additional analysis performed on sections from patients 3 and 4 biopsies, carrying the p.(Gly103Asp) and the p.(Ile385Thr) mutations, respectively, revealed that additional SR proteins such as CASQ1, RYR1 and STIM1 were present in the aggregates (Figure 2). ORAI1 was usually not detectable in CASQ1-positive tubular aggregrates or only at much lower levels (Figure 2).

All the variants identified affect amino acid residues conserved across species (Figure 1C). Two of the variants identified in TAM patients are reported in the ExAC exome database (exac.broadinstitute.org) as rs140253806 (c.130G > A) and rs371278891 (c.1154 T > C) with a minor allele frequency established of 0.002 and 0.00011, respectively. It is worth noting that the frequency of these variants, being higher than that reported for TAM cases, may reflect an underdiagnosis of TAM in the general population and/or that some individuals might be asymptomatic carrier, thus making it difficult to determine the real frequency of this disorder. The other variant, c.308G > A, has not been described, although two distinct rare substitutions affecting the same codon (rs567336006) have been reported. Damage prediction on protein function was assessed using established online tools (SIFT [https://sift.bii.a-star.edu.sg/index.html] and Polyphen-2 [https://genetics.bwh.harvard.edu/pph2/index.shtml]). This analysis indicated the p.(Asp44Asn) substitution as deleterious (SIFT: 0.0; PolyPhen2: 1.0). SIFT and PolyPhen2 analysis indicated the p.(Gly103Asp) and p.(Ile385Thr) as tolerated (SIFT: 0.553; PolyPhen2: 0.007 and SIFT: 0.117; PolyPhen2: 0.593, respectively). These predictions are based exclusively on the CASQ1 sequence and on the degree of amino acid residues conservation in closely related sequence alignments. The effects of these mutations on the tertiary structure as well as possible consequences on polymeric forms of the protein are not considered. To exclude mutations in other genes, WES was performed on the four patients. No mutations were detected in *STIM1* and *ORAI1* genes. Moreover, variants were filtered for a frequency $\leq$ 0.001, shared among the affected individuals and not present in five healthy controls. This analysis revealed no other potentially pathological variants in the four probands. The position of these three TAM mutations is reported in Figure 1D, along with that of the p(Asp244Gly) mutation identified in patients with vacuolar aggregate myopathy, using a model of polymerization based on the crystal structures of WT and p.Asp244Gly CASQ1 (Lewis, Ronish, Ríos, & Kang, 2015; Wang et al., 1998). Interestingly, these mutations are located at sites of back-to-back (p.Asp244Gly and p.Ile385Thr) or front-to-front interactions (p.Asp44Asn and p.Gly103Asp).

3.2 | p.Asp44Asn and p.Gly103Asp proteins are more susceptible to proteolysis

Proteases can be used at low concentrations to distinguish folded from unfolded proteins, based on the observation that unfolded proteins are cut more rapidly than structured proteins due to the inability of proteases to access buried sites. To investigate CASQ1
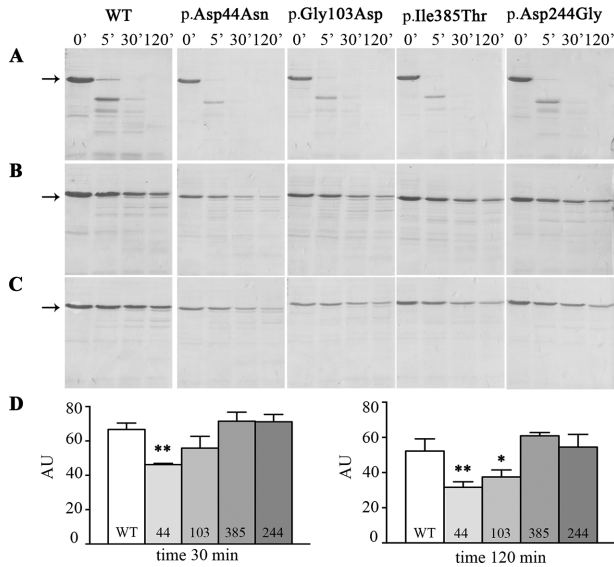
FIGURE 3 Limited trypsin proteolysis assay. WT CASQ1 and mutants were subjected to proteolysis in the absence of Ca^{2+} (**A**), in the presence of 1 mM Ca^{2+} (**B**) or 3 mM Ca^{2+} (**C**). **D**: Densitometric analysis of the intact protein (arrows) at 30 and 120 min of trypsin incubation, in presence of 1 mM Ca^{2+}. P values ≤0.05 and 0.005 are indicated by * and **, respectively. Experiments were repeated three times

proteins conformation/aggregation at increasing Ca^{2+} concentrations, recombinant CASQ1 proteins containing the three different TAM mutations were purified from bacteria together with the WT and the p.Asp244Gly previously reported in vacuolar aggregate myopathy (Di Blasi et al., 2015; Rossi et al., 2014b). CASQ1 aggregation propensity was analyzed by limited trypsin proteolysis in absence or presence of increasing Ca^{2+} concentrations. In the absence of Ca^{2+}, all proteins were highly sensitive to trypsin digestion. The addition of Ca^{2+} reduced the proteolysis of WT and mutated CASQ1 proteins demonstrating appropriate changes in the aggregation state of these proteins. Densitometric analysis of the intact protein at 0 min (input) compared with the different trypsin incubation times revealed, at 1 and 3 mM Ca^{2+}, that p.Asp44Asn and p.Gly103Asp remained more susceptible to trypsin proteolysis, although this tendency decreased for p.Gly103Asp. No differences were detected for the p.Ile385Thr and p.Asp244Gly mutations. In particular, in presence of 1 mM Ca^{2+}, the amount of residual p.Asp44Asn was 46% and 32% and the amount of residual p.Gly103Asp was 56% and 37%, whereas WT displayed a maximum value of residual protein of 67% and 52% at 30 and 120 min of incubation, respectively (Figure 3).

3.3 | TAM-associated CASQ1 mutations show altered Ca^{2+}-induced aggregation properties

To study the aggregation properties of the CASQ1 mutants, turbidity measurements were performed exposing purified CASQ1 proteins to increasing Ca^{2+} concentrations and measuring the absorbance at 350 nm. Increasing absorbance was detected with WT CASQ1 across the tested Ca^{2+} concentrations, as expected. The p.Asp244Gly mutation aggregated more than WT, displaying an increase in absorbance
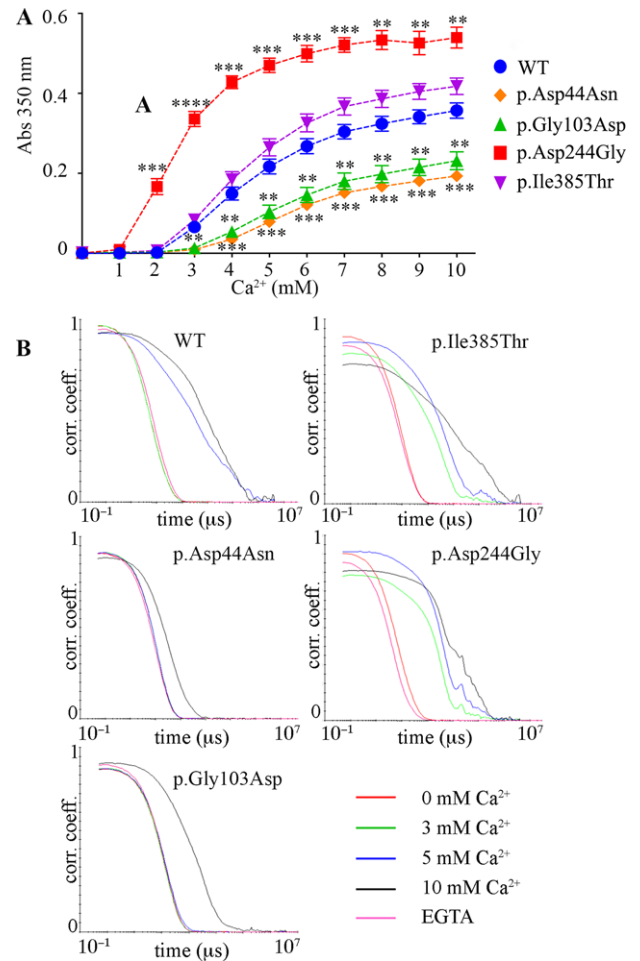

FIGURE 4 Ca^{2+}-dependent aggregation of purified CASQ1 proteins. **A**: CASQ1 turbidity is measured as absorbance at 350 nm (blue circle, WT; orange diamond, p.Asp44Asn; green triangle, p.Gly103Asp; red square, p.Asp244Gly; violet inverted triangle, p.Ile385Thr). Experiments were carried out in a buffer containing 20 mM Tris–HCl, 150 mM KCl (pH 7.4), and 0–10 mM Ca^{2+}. Data are presented as mean ± SEM and statistical analysis versus WT was performed by two-tailed unpaired Student's test. P values ≤0.005 and 0.0005 are indicated by ** and ***, respectively. **B**: DLS measured correlation curves at increasing Ca^{2+} concentrations (red, 0; green, 3; blue, 5; and black, 10 mM Ca^{2+}) for WT and CASQ1 mutants. The right-shifting of the profiles to higher correlation times is correlated to the increase in the mean size of the samples, that is, to the formation of aggregates. In absence of Ca^{2+}, the correlograms are very similar for the five samples, indicating a similar initial state. In all cases, the aggregation process induced by Ca^{2+} is reversible as indicated by the effect of the addition of 10 mM EGTA

that started between 1 and 2 mM Ca^{2+} and that remained higher until 10 mM Ca^{2+}, in agreement with reported data (Lewis et al., 2015). TAM-associated CASQ1 mutations have a different behavior compared with WT and p.Asp244Gly. The p.Ile385Thr mutant showed an increase in turbidity consistently higher, although not significantly different from WT. On the contrary, turbidity values observed between 1 and 10 mM Ca^{2+} with both p.Gly103Asp and p.Asp44Asn were constantly lower than WT (Figure 4A). All aggregations were fully reversed by the addition of EGTA (not shown).

The Ca^{2+}-dependent aggregation tendency of the proteins was also evaluated by DLS, a technique highly sensitive to the presence of aggregates as the signal depends on the hydrodynamic properties of the scattering object in solution and hence on its dimensions (both size and shape). As shown in Figure 4B, WT protein did not appreciably change its aggregation state between 0 and 3 mM Ca^{2+}. At 5 mM Ca^{2+}, the signal revealed a more aggregated sample and at 10 mM Ca^{2+} the sample appeared even more aggregated. The p.Asp244Gly mutation had the highest tendency to aggregate, showing aggregation already at 3 mM Ca^{2+}, with the correlogram shifted to higher correlation times. The mutation p.Ile385Thr showed a similar behavior, starting aggregating from 3 mM Ca^{2+} on. In contrast, mutations p.Gly103Asp and p.Asp44Asn did not change their aggregation state up to 5 mM Ca^{2+} and were found aggregated only at 10 mM Ca^{2+}. With all proteins, aggregation was fully reversed by the addition of EGTA.

3.4 | Single muscle fibers from patient with the p.Gly103Asp mutation show altered response to caffeine stimulation

To correlate SR alterations to the myopathic phenotype, the tension elicited by stimulation with increasing concentrations of caffeine was studied in single muscle fibers isolated from a biopsy of patient 3 (p.Gly103Asp) and compared with fibers dissected from four healthy subjects of comparable age, as described in *Materials and Methods.* Examples of response to 2 mM and 20 mM caffeine are given in Figure 5A: the response induced by 2 mM caffeine (Figure 5A1 and A3) and by 20 mM caffeine (Figure 5A2 and A4) were much lower in a fiber of the patient 3 (Figure 5A3 and A4) compared with a fiber of a control subject (Figure 5A1 and A2). As can be seen in Figure 5B, average dose–response curves show that the maximal response was significantly reduced in a balanced pool of fast and slow fibers of the patient 3 in comparison with healthy control fibers of comparable age, although the responsiveness to caffeine measured as log EC50% was not reduced.

3.5 | Altered Ca^{2+} handling in HeLa cells expressing CASQ1 mutations

To directly analyze the ability of CASQ1 mutations to increase the ER Ca^{2+} storage capability, the WT and CASQ1 mutations were expressed in HeLa cells and intracellular Ca^{2+} levels were measured following Fura-2 loading. Transfected cells were treated with Tg to measure the total content of Ca^{2+} in the ER. Expression of WT CASQ1 increased the intracellular Ca^{2+} content, as expected (Figure 5C and D). Transfection of the three novel TAM-associated mutations and of the p.Asp244Gly, responsible for vacuolar aggregate myopathy, resulted in a significant lower increase in the amount of Tg-releasable Ca^{2+} revealing that all CASQ1 mutants analyzed have a reduced ability in increasing the intracellular Ca^{2+} store content compared to WT CASQ1. Earlier work has shown that CASQ expression has an inhibitory effect on the pathways that regulate SOCE, the mechanism needed to refill intracellular Ca^{2+} store in eukaryotic cells (Shin et al., 2003; Wang et al., 2015; Zhao et al., 2010). Therefore, we measured the peak phase following the

addition of extracellular Ca^{2+} to measure the amount of Ca^{2+} entering cells after emptying stores with Tg (Figure 5E and F). In agreement with reported data, following addition of 1.5 mM extracellular Ca^{2+}, expression of WT CASQ1 inhibited SOCE. However, under these conditions, the expression of the TAM-associated p.Asp44Asn and p.Ile385Thr mutations did not result in a significant reduction of Ca^{2+} influx, suggesting a reduced ability to inhibit SOCE. On the contrary, expression of the p.Gly103Asp mutation found in TAM patients and of the p.Asp244Gly mutation, found in patients with vacuolar aggregate myopathy, resulted in an inhibition of Ca^{2+} influx comparable to that obtained with WT CASQ1.

3.6 | Expression of WT and mutant CASQ1 proteins does not affect the subcellular localization of STIM1 in transfected cells

CASQ1 was reported to inhibit SOCE by preventing STIM1 aggregation (Zhang et al., 2016). We thus investigated the effects of CASQ1 mutants on STIM1 clusters assembly. HeLa cells were co-transfected with expression plasmids encoding mRFP-STIM1 and GFP fusion proteins of WT or mutant CASQ1. Cells were treated with 1 μM Tg to induce activation of SOCE. STIM1 aggregation and CASQ1 depolymerization were analyzed by live imaging confocal microscopy on four to five focal planes to image the cortical ER close to the plasma membrane and the regular ER positioned in the interior of the cell (Supp. Figure S2). Under resting conditions, WT CASQ1-GFP formed linear and round aggregates in the ER, which reflect the assembly of large CASQ1 polymers at physiological Ca^{2+} concentration, while in a minority of cells CASQ1 proteins were more homogeneously diffused in the ER lumen (Supp. Table S1). Similarly, transfection of the p.Asp44Asn-GFP, p.Gly103Asp-GFP, and p.Ile385Thr-GFP mutants resulted in the assembly of linear aggregates and clusters, with a remaining fraction of cells showing a CASQ1-GFP signal diffused in the ER. In contrast, expression of the p.Asp244Gly-GFP protein resulted in assembly of round aggregates in the majority of the cells, with only a minor fraction of cells showing linear polymers (Supp. Table S1). Imaging of the mRFP-STIM1 in these cells resulted in fluorescence signal compatible with ER localization, both in cells expressing WT and mutant CASQ1, thus showing no co-localization with the linear and round aggregates of CASQ1 (Supp. Figure S2).

Following treatment with Tg, the linear structures formed by WT CASQ1 as well as p.Asp44Asn and p.Ile385thr mutants disappeared and the GFP fluorescence signal redistributed to the ER and, to a lesser extent, in round aggregates. At variance, linear aggregates formed by the p.Gly103Asp mutant disappeared and the signal was mainly found in round clusters and to a lesser extent diffused in the ER. Finally, the distribution of p.Asp244Gly did not significantly change following Tg treatment, suggesting a reduced ability of this protein to depolymerize (Supp. Figure S2). In parallel, the formation of STIM1 clusters at the plasma membrane was analyzed in cells co-expressing WT and mutant CASQ1. Measurement of the average size of STIM1 clusters formed following Tg treatment showed that clusters assembled in cells expressing WT or p.Asp244Gly were apparently larger compared to those measured in cells expressing mutants p.Asp44Asn, p.Gly103Asp,
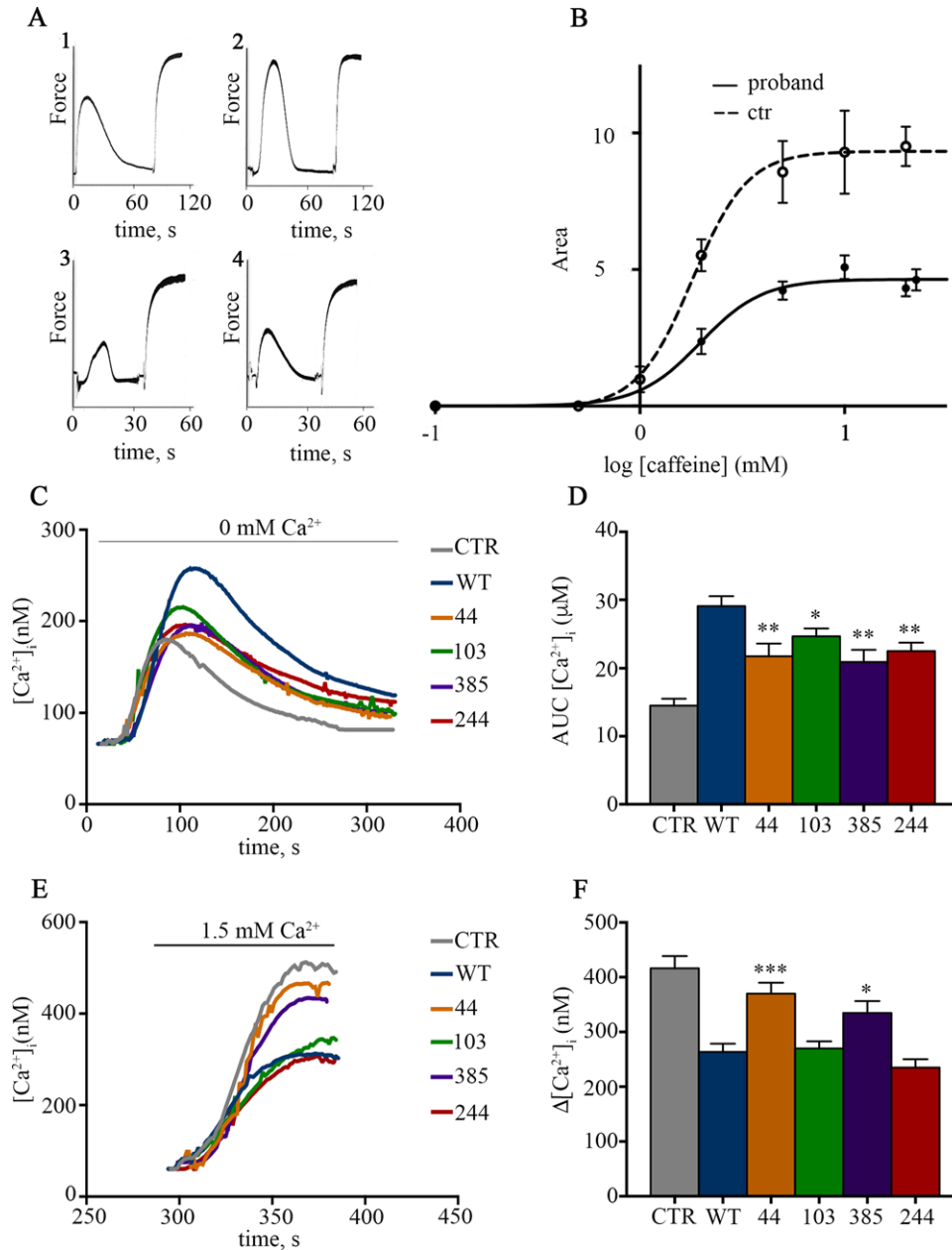
FIGURE 5 Response to caffeine of muscle fibers of patient 3 and analysis of intracellular Ca^{2+} stores and Ca^{2+} entry in HeLa cells expressing WT and mutant CASQ1. **A**: Response to caffeine of muscle fibers from patient 3 and from healthy controls. Examples of fibers response to the administration of 2 mM caffeine (panels 1 and 3: control and patient 3, respectively) and 20 mM caffeine (2 and 4: control and patient 3, respectively). Each release induced a wave of contraction, whose amplitude was expressed as tension-time area and was normalized to the amplitude of the response induced by maximal direct activation with pCa 4.3. The greater amplitude of the response induced by a given concentration of caffeine in control (panels 1 and 2) compared with patient 3 (panels 3 and 4) is clearly detectable. **B**: Caffeine dose–response curves of permeabilized muscle fibers from control healthy subjects (black dashed line, open circles) and patient 3 (continuous black line, filled circles). Contraction, analyzed as an indirect measure of Ca^{2+} release, was induced by concentrations of caffeine in the range from 0.1 to 20 mM (expressed in logarithmic scale). Curves were interpolated by a sigmoidal Hill equation: $Y = B + \{(A_{max} - B)/(1 + 10\hat{}([\log EC_{50} - X]*n)\}$. **C**: Representative traces of Ca^{2+} release from intracellular stores of HeLa cells untransfected (CTR) or transfected with WT or different CASQ1 mutations and loaded with Fura-2 following treatment with Thapsigargin (Tg) in the absence of extracellular Ca^{2+}. **D**: Quantification of Ca^{2+} release. Mean values $\pm$ SEM of area under the curve (AUC) measurements were calculated from traces of all experiments. **E**: Representative traces of Ca^{2+} influx from single cells evoked by the re-admission of 1.5 mM Ca^{2+} in HeLa cells pre-treated with Tg. **F**: Quantification of Ca^{2+} influx. Bars indicate $\Delta[Ca^{2+}]_I$ (nM) $\pm$ SEM. Data presented in panels D and F are from 172, 166, 99, 260, 130, and 141 cells for CTR, WT, and p.Asp44Asn, p.Gly103Asp, p.Ile385Thr, and p.Asp244Gly mutants, respectively. Measurements were obtained from at least 16 independent experiments. Data are mean $\pm$ SEM and statistical evaluation of the data in D and F was performed by the two-tailed unpaired Student's test with systematic Welch correction for variance. Statistically significant differences versus WT are indicated by * (P values $\leq$ 0.05), ** (P values $\leq$ 0.005) and *** (P values $\leq$ 0.0005)

and p.Ile385Thr, although statistical analysis did not reveal significant differences (Supp. Table S2). Analysis of top to bottom focal planes acquired in resting conditions and following Tg treatment showed that the mRFP-STIM1 fluorescence signal progressively increased from median to top focal planes resembling the assembly of cortical ER structures induced by Ca^{2+} store depletion and SOCE activation. On the contrary, the GFP-CASQ1 fluorescence signal did not apparently follow the assembly of cortical ER structures and remained mainly in median planes even at the end of Tg treatment (Suppl. Figure S2). No significant co-localization between STIM1 and WT and CASQ1 mutants before and after Tg treatment was detected by Pearson coefficient analysis.

4 | DISCUSSION

Here, we report the first identification and characterization of three missense mutations in the *CASQ1* gene in four unrelated patients with TAM with diffuse myalgia, post-exercise fatigue, and typical cytoplasmic tubular aggregates. Until now, only mutations in *STIM1* and *ORAI1* have been identified in patients with TAM. The TAM patients with CASQ1 mutations have a milder phenotype compared with TAM patients with mutations in STIM1 and ORAI1 and to patients with vacuolar aggregate myopathy, a related disorder that is caused by a different mutation in CASQ1. No one of the TAM patients carrying mutations in CASQ1 presented additional signs related to Stormorken syndrome. Functional characterization of these CASQ1 mutations revealed altered polymerization tendency and a common reduced ability to increase intracellular Ca^{2+} stores. However, the ability of CASQ1 mutations to inhibit Ca^{2+} entry pathways was maintained in only one of the three mutations, suggesting a further potential level of complexity in the pathomechanisms of TAM due to mutations in *CASQ1*.

4.1 | CASQ1 mutations are localized at sites of interactions between CASQ1 subunits

The extraordinary ability of CASQ1 to bind Ca^{2+} with high-capacity appears to depend on its propensity to form large polymers in a highly regulated, Ca^{2+}-dependent process. Indeed, the current model for CASQ1 polymerization indicates that low concentrations of Ca^{2+} induce formation of dimers by favoring front-to-front interactions between monomers, while increasing Ca^{2+} concentrations result in the assembly of tetramers, through back-to-back interactions, which will then result in large, complex CASQ1 polymers that contain additional Ca^{2+} binding sites at the interface between CASQ1 dimers and tetramers (Kumar et al., 2013, Park et al., 2003). Initial studies on the p.Asp244Gly revealed an extremely rapid aggregation and a significant reduction of the Ca^{2+} binding properties of this protein (Lewis et al., 2015). We observed altered aggregation ability in all three CASQ1 mutations identified in patients with TAM. Aggregation of the p.Ile385Thr mutation was more sensitive to Ca^{2+} than WT CASQ1, even if much less than the p.Asp244Gly mutation. In contrast, both p.Asp44Asn and p.Gly103Asp mutations were less susceptible to aggregate at rising Ca^{2+} concentrations than WT CASQ1, similarly to

what reported for the p.Met87Thr mutation (Lewis et al., 2015). Using the available crystal structures of WT and p.Asp244Gly CASQ1 (Lewis et al., 2015; Wang et al., 1998), we noticed the three CASQ1 mutations identified in TAM patients are located at sites that can affect the interactions between CASQ1 subunits. Initial studies with the p.Asp244Gly mutation (Lewis et al., 2015) indicated that it may decrease the association of dimers through linear back-to-back interactions. As shown in Figure 1D, the p.Ile385Thr mutation is located at the interface of "lateral" back-to-back contacts that are responsible for the formation of the branched polymers formed by WT CASQ1 (Perni, Close, & Franzini-Armstrong, 2013). Moreover, the negatively charged C-terminal tail, immediately downstream of Ile385, has been shown to be important to hamper the formation of not-specific polymerization products (Beard & Dulhunty, 2015; Park et al., 2004). Hence, it can be hypothesized that the p.Ile385Thr mutation favors the assembly of atypical, not-fully functional, polymeric forms. On the other hand, residues 44 and 103 are positioned at the interface responsible for the formation of CASQ1 dimers (Figure 1D and Supp. Figure S1). Accordingly, the p.Asp44Asn and p.Gly103Asp mutations can affect the interactions that strengthen the front-to-front dimerization of the protein, resulting in dimers less efficient in supporting the formation of back-to-back tetramers, similarly to what proposed for the p.Met87Thr mutation (Lewis et al., 2015; Supp. Figure S1). It can be noted that the CASQ1 mutations that have increased polymerization (p.Asp244Gly and p.Ile385Thr) are located at sites of back-to-back interactions, while CASQ1 mutations that have a reduced polymerization (p.Asp44Asn and p.Gly103Asp) are positioned at sites of front-to-front interactions.

4.2 | CASQ1 mutations impair intracellular Ca^{2+} homeostasis

Analysis of single muscle fibers isolated from patient 3, carrying the p.Gly103Asp mutation, revealed a significant reduction in tension developed following maximal stimulation with caffeine, a result that suggests a possible reduced ability to store Ca^{2+} in these fibers. Indeed, all three TAM CASQ1 mutations, when transfected in HeLa cells, showed a reduced ability to increase the intracellular Ca^{2+} store content compared with WT CASQ1. Given that either increased or decreased polymerization tendency may reduce the ability of CASQ1 to bind Ca^{2+}, we hypothesize that the altered polymerization properties of the TAM CASQ1 mutations may explain their reduced capacity to enhance intracellular Ca^{2+} stores in muscle fibers and in transfected cells.

CASQ1 has been shown to inhibit SOCE by interacting with STIM1 and by reducing STIM1 aggregation (Wang et al., 2015; Zhang et al., 2016). Surprisingly, we observed different effects among the TAM CASQ1 mutations on the mechanisms of Ca^{2+} entry. Indeed, p.Asp44Asn and p.Ile385Thr showed loss of the ability to inhibit Ca^{2+} influx, while p.Gly103Asp presented an inhibitory effect similar to that of WT and of p.Asp244Gly. The observed effects on Ca^{2+} influx did not correlate with Ca^{2+}-induced polymerization ability, or trypsin resistance, or ability to increase intracellular Ca^{2+} stores of the CASQ1 mutations (Supp. Table S3). It is worth noting that the observed increase in total Ca^{2+} content observed in transfected cells expressing

WT or CASQ1 mutants is due to Ca^{2+} bound to CASQ1 in the SR, thus it should not affect intracellular levels of free Ca^{2+} or influence SOCE (Rios, 2010). In spite of the contrasting effects on SOCE observed with WT and mutant CASQ1 proteins, we did not notice significant differences between expression of WT and mutant CASQ1 proteins on STIM1 localization and aggregation before or after Tg treatment. Altogether, these data suggest that changes in the ability to inhibit SOCE might not be an obligatory event in the pathogenic mechanism of TAM-associated CASQ1 mutations, at variance with the mechanisms of disease for TAM- associated mutations in *STIM1* and *ORAI1*. It is possible that identification of more subtle changes in the properties of CASQ1 mutants may help to understand the mechanisms whereby CASQ1 inhibits SOCE. Additional studies are needed to further address this point.

4.3 | CASQ1 mutations in TAM and vacuolar aggregate myopathy

Although the exact mechanisms responsible for inducing tubular aggregates formations are not fully understood, it is currently accepted that these structures may result from proliferation of the SR membrane triggered by conditions of ER stress due, among other causes, to misfolding of SR proteins resulting in the formation of protein aggregates and/or by altered Ca^{2+} homeostasis (Chevessier et al., 2005; Schiaffino, 2012). The results reported here indicate that, similar to mutations in *STIM1* and *ORAI1*, TAM-associated CASQ1 mutations can also affect intracellular Ca^{2+} homeostasis. It is therefore possible that the SR proteins aggregates observed in the biopsies of TAM patients may result as a consequence of impaired Ca^{2+} homeostasis or of the modified polymerization properties of CASQ1 mutations, or of a combined effect of the two.

TAM patients with CASQ1 mutations refer symptoms like diffuse myalgia, muscle weakness, post-exercise fatigue, and, at the histological level, present typical aggregates of membrane tubules in type II fibers. Patients with vacuolar aggregate myopathy, who all carry the p.Asp244Gly *CASQ1* mutation, in addition to the symptoms described above for TAM patients with CASQ1 mutations, report also cramps and, more frequently, present elevated plasma creatine kinase levels. At the histological level, the distinctive hallmark of vacuolar aggregate myopathy are large vacuoles containing compact electron-dense inclusions of variable size and shape, that do not stain with several routine histochemical techniques, like the NADH reaction, which in contrast stains tubular aggregates.

All three *CASQ1* mutations identified in TAM patients have either a mild increase in Ca^{2+}-dependent polymerization ability (p.Ile385Thr) or are less able to polymerize than WT CASQ1 (p.Asp44Asn and p.Gly103Asp). This differs from the property of the p.Asp244Gly mutation that shows a strong increase in Ca^{2+}-dependent polymerization (Lewis et al., 2015). The p.Asp244Gly mutation also displays a reduced ability to increase intracellular Ca^{2+} store content, a property common to all CASQ1 TAM mutations analyzed, and an inhibitory effect on SOCE similar to that of WT and p.Gly103Asp mutation. Interestingly, all TAM CASQ1 mutations can form elongated polymers, similar to those formed by WT CASQ1, that differ in their

structure and dynamics properties from the aggregated polymers formed by the p.Asp244Gly mutation (Rossi et al., 2014b and Supp. Figure S1). Thus, the major difference between p.Asp244Gly and the TAM CASQ1 mutations is represented by its exaggerated tendency to aggregate in irregular CASQ1 polymers (Lewis et al., 2015; Rossi et al., 2014b). Accordingly, we hypothesize that the large vacuoles of several μm in diameter that represent the hallmark of vacuolar aggregate myopathy (Tomelleri et al., 2006) develop as a result of the large dimensions of the p.Asp244Gly aggregates that, given their size, cannot be accommodated within the lumen of tubular aggregates, which usually have a diameter of 60–100 nm, and only more rarely of 200–400 nm.

5 | CONCLUSIONS

We report here the discovery of three novel missense mutations in the *CASQ1* gene in four unrelated patients with TAM. These findings identify *CASQ1* as a new gene responsible for inducing TAM, in addition to *STIM1* and *ORAI1*. Characterization of these mutations indicated that they all modify the polymerization properties of CASQ1 and have a reduced ability to increase intracellular Ca^{2+} stores, compared with WT CASQ1. A reduction in caffeine response, which also points to reduced intracellular Ca^{2+} stores content, was also observed in fibers form a patient carrying the p.(Gly103Asp) mutation. We propose that altered polymerization ability of the CASQ1 mutations diminish their capacity to attain maximal Ca^{2+} binding and this might explain the decreased Ca^{2+} content of intracellular stores. Less clear remains, at the moment, the relationship between the above reported properties and the various effects of CASQ1 mutation on Ca^{2+} entry. More work will help to better understand the multiple mechanisms operated by CASQ1 in maintaining physiological skeletal muscle Ca^{2+} homeostasis and function, and how mutations in *CASQ1* modify these mechanisms in TAM and vacuolar aggregate myopathy.

ORCID

Vincenzo Sorrentino (ID) http://orcid.org/0000-0002-8573-8631

REFERENCES

Agbulut, O., Destombes, J., Thiesson, D., & Butler-Browne, G. (2000). Age-related appearance of tubular aggregates in the skeletal muscle of almost all male inbred mice. *Histochemistry and Cell Biology*, 114, 477–481.

Barone, V., Randazzo, D., Del Re, V., Sorrentino, V., & Rossi, D. (2015). Organization of junctional sarcoplasmic reticulum proteins in skeletal muscle fibers. *Journal of Muscle Research and Cell Motility*, 36, 501–515.

Beard, N. A., & Dulhunty, A. F. (2015). C-terminal residues of skeletal muscle calsequestrin are essential for calcium binding and for skeletal ryanodine receptor inhibition. *Skeletal Muscle*, 5, 6–18.

Bertoldi, L., Forcato, C., Vitulo, N., Birolo, G., De Pascale, F., Feltrin, E., … Valle, G. (2017). QueryOR: A comprehensive web platform for genetic variant analysis and prioritization. *BMC Bioinformatics*, 18, 225–236.

Böhm, J., Chevessier, F., De Paula, A. M., Koch, C., Attarian, S., Feger, C., … Laporte, J. (2013). Constitutive activation of the calcium sensor STIM1 causes tubular-aggregate myopathy. *American Journal of Human Genetics*, 92, 271–278.

Böhm, J., Chevessier, F., Koch, C., Peche, G. A., Mora, M., Morandi, L., … Laporte, J. (2014). Clinical, histological and genetic characterisation of patients with tubular aggregate myopathy caused by mutations in STIM1. *Journal of Medical Genetics*, 51, 824–833.

Böhm, J., Bulla, M., Urquhart, J. E., Malfatti, E., Williams, S. G., O'Sullivan, J., … Laporte, J. (2017). ORAI1 mutations with distinct channel gating defects in tubular aggregate myopathy. *Human Mutation*, 38, 426–438.

Boncompagni, S., Protasi, F., & Franzini-Armstrong, C. (2012). Sequential stages in the age-dependent gradual formation and accumulation of tubular aggregates in fast twitch muscle fibers: SERCA and calsequestrin involvement. *Age (Dordrecht)*, 34(1)27–41.

Chevessier, F., Bauche-Godard, S., Leroy, J. P., Koenig, J., Paturneau-Jouas, M., Eymard, B., … Verdiere-Sahuque, M. (2005). The origin of tubular aggregates in human myopathies. *Journal of Pathology*, 207, 313–323.

Di Blasi, C., Sansanelli, S., Ruggieri, A., Moriggi, M., Vasso, M., D'Adamo, A. P., … Mora, M. (2015). A CASQ1 founder mutation in three italian families with protein aggregate myopathy and hyperCKaemia. *Journal of Medical Genetics*, 52, 617–626.

Doria, C., Toniolo, L., Verratti, V., Cancellara, P., Pietrangelo, T., Marconi, V., … Capelli, C. (2011). Improved VO2 uptake kinetics and shift in muscle fiber type in high altitude trekkers. *Journal of Applied Physiology*, 111, 1597–1605.

Endo, M., & Iino, M. (1988). Measurement of Ca^{2+} release in skinned fibers from skeletal muscle. *Methods in Enzymology*, 157, 12–26.

Endo, Y., Noguchi, S., Hara, Y., Hayashi, Y. K., Motomura, K., Miyatake, S., … Nishino, I. (2015). Dominant mutations in ORAI1 cause tubular aggregate myopathy with hypocalcemia via constitutive activation of store-operated Ca^{2+} channels. *Human Molecular Genetics*, 24, 637–648.

Engel, W. K., Bishop, D. W., & Cunningham, G. G. (1970). Tubular aggregates in type II muscle fibers: Ultrastructural and histochemical correlation. *Journal of Ultrastructure Research*, 31, 507–525.

Faggioni, M., Kryshtal, D. O., & Knollmann, B. C. (2012). Calsequestrin mutations and catecholaminergic polymorphic ventricular tachycardia. *Pediatric Cardiology*, 33, 959–967.

Feske, S., Gwack, Y., Prakriya, M., Srikanth, S., Puppel, S. H., Tanasa, B., … Rao, A. (2006). A mutation in Orai1 causes immune deficiency by abrogating CRAC channel function. *Nature*, 441, 179–185.

Fryer, M. W., & Stephenson, D. G. (1996). Total and sarcoplasmic reticulum calcium contents of skinned fibres from rat skeletal muscle. *Journal of Physiology*, 493, 357–370.

Giacomello, E., Quarta, M., Paolini, C., Squecco, R., Fusco, P., Toniolo, L., … Sorrentino, V. (2015). Deletion of small ankyrin 1 (sAnk1) isoforms results in structural and functional alterations in aging skeletal muscle fibers. *American Journal of Physiology—Cell Physiology*, 308, C123–C138.

Giurisato, E., Gamberucci, A., Ulivieri, C., Marruganti, S., Rossi, E., Giacomello, E., … Sorrentino, V. (2014). The KSR2-calcineurin complex regulates STIM1-ORAI1 dynamics and store-operated calcium entry (SOCE). *Molecular Biology of the Cell*, 25, 1769–1781.

Kumar, A., Chakravarty, H., Bal, N. C., Balaraju, T., Jena, N., Misra, G., … Sharon, A. (2013). Identification of calcium binding sites on calsequestrin-1 and their implications for polymerization. *Molecular Biosystems*, 9, 1949–1957.

Kuncl, R. W., Pestronk, A., Lane, J., & Alexander, E. (1989). The MRL +/+ mouse: A new model of tubular aggregates which are gender- and age-related. *Acta Neuropathology*, 78, 615–620.

Lacruz, R. S., & Feske, S. (2015). Diseases caused by mutations in *ORAI1* and *STIM1*. *Annals of the New York Academy of Sciences*, 356, 45–79.

Lahat, H., Pras, E., Olender, T., Avidan, N., Ben-Asher, E., Man, O., … Eldar, M. (2001). A missense mutation in a highly-conserved region of CASQ2 is associated with autosomal recessive catecholamine-induced polymorphic ventricular tachycardia in Bedouin families from Israel. *American Journal of Human Genetics*, 69, 1378–1384.

Lamb, G. D., Cellini, M. A., & Stephenson, D. G. (2001). Different Ca^{2+} releasing action of caffeine and depolarisation in skeletal muscle fibres of the rat. *Journal of Physiology*, 531, 715–728.

Lamboley, C. R., Wyckelsma, V. L., Dutka, T. L., McKenna, M. J., Murphy, R. M., & Lamb, G. D. (2015). Contractile properties and sarcoplasmic reticulum calcium content in type I and type II skeletal muscle fibres in active aged humans. *Journal of Physiology*, 593, 2499–2514.

Lewis, K. M., Ronish, L. A., Ríos, E., & Kang, C. (2015). Characterization of two human skeletal calsequestrin mutants implicated in malignant hyperthermia and vacuolar aggregate myopathy. *Journal of Biological Chemistry*, 290, 28665–28674.

Makabe, M., Werner, O., & Fink, R. H. (1996). The contribution of the sarcoplasmic reticulum Ca^{2+}-transport ATPase to caffeine-induced Ca2+ transients of murine skinned skeletal muscle fibres. *Pflugers Archiv*, 432, 717–726.

Maus, M., Jairaman, A., Stathopulos, P. B., Muik, M., Fahrner, M., Weidinger, C., … Feske, S. (2015). Missense mutation in immunodeficient patients shows the multifunctional roles of coiled-coil domain 3 (CC3) in STIM1 activation. *Proceedings of the National Academy of Sciences of the United States of America*, 112, 6206–6211.

Misceo, D., Holmgren, A., Louch, W. E., Holme, P. A., Mizobuchi, M., Morales, R. J., … Frengen, E. (2014). A dominant STIM1 mutation causes Stormorken syndrome. *Human Mutation*, 35, 556–564.

Nesin, V., Wiley, G., Kousi, M., Ong, E. C., Lehmann, T., Nicholl, D. J., … Tsiokas, L. (2014). Activating mutations in STIM1 and ORAI1 cause overlapping syndromes of tubular myopathy and congenital miosis. *Proceedings of the National Academy of Sciences of the United States of America*, 111, 4197–4202.

Okuma, H., Saito, F., Mitsui, J., Hara, Y., Hatanaka, Y., Ikeda, M., … Sonoo, M. (2016). Tubular aggregate myopathy caused by a novel mutation in the cytoplasmic domain of STIM1. *Neurology: Genetics*, 2, e50–e57.

Park, H., Wu, S., Dunker, A. K., & Kang, C. (2003). Polymerization of calsequestrin. Implications for Ca^{2+} regulation. *Journal of Biological Chemistry*, 278, 16176–16182.

Park, H., Park, I. Y., Kim, E., Youn, B., Fields K. A., Dunker, K. A., & ChulHee Kang, C. (2004). Comparing skeletal and cardiac calsequestrin structures and their calcium binding. *Journal of Biological Chemistry*, 279, 18026–18033.

Perni, S., Close, M., & Franzini-Armstrong, C. (2013). Novel details of calsequestrin gel conformation in situ. *Journal of Biological Chemistry*, 288, 31358–31362.

Rios, E. (2010). The cell boundary theorem: A simple law of the control of cytosolic calcium concentration. *Journal of Physiological Sciences*, *60*, 81–84.

Rossi, R., Bottinelli, R., Sorrentino, V., & Reggiani, C. (2001). Response to caffeine and ryanodine receptor isoforms in mouse skeletal muscles. *American Journal of Physiology—Cell Physiology*, *281*, C585–C594.

Rossi, D., Bencini, C., Maritati, M., Benini, F., Lorenzini, S., Pierantozzi, E., … Sorrentino, V. (2014a). Distinct regions of triadin are required for targeting and retention at the junctional domain of the sarcoplasmic reticulum. *Biochemical Journal*, *458*, 407–417.

Rossi, D., Vezzani, B., Galli, L., Paolini, C., Toniolo, L., Pierantozzi, E., … Sorrentino, V. (2014b). A mutation in the CASQ1 gene causes a vacuolar myopathy with accumulation of sarcoplasmic reticulum protein aggregates. *Human Mutation*, *35*, 1163–1170.

Salviati, G., Pierobon-Bormioli, S., Betto, R., Damiani, E., Angelini, C., Ringel, S. P., … Margreth, A. (1985). Tubular aggregates: Sarcoplasmic reticulum origin, calcium storage ability, and functional implications. *Muscle Nerve*, *8*, 299–306.

Salviati, G., & Volpe, P. (1988). Ca^{2+} release from sarcoplasmic reticulum of skinned fast- and slow-twitch muscle fibers. *American Journal of Physiology*, *254*, C459–C465.

Sanchez, E. J., Lewis, K. M., Danna, B. R., & Kang, C. (2012). High-capacity Ca^{2+} binding of human skeletal calsequestrin. *Journal of Biological Chemistry*, *287*, 11592–11601

Scherer, T. M., Leung, S., Owyang, L., & Shire, S. J. (2012). Issues and Challenges of subvisible and submicron particulate analysis in protein solutions. *AAPS Journal*, *14*, 236–243.

Schiaffino, S., & Reggiani, C. (2011). Fiber types in mammalian skeletal muscles. *Physiological Reviews*, *91*, 1447–1531.

Schiaffino, S. (2012). Tubular aggregates in skeletal muscle: Just a special type of protein aggregates? *Neuromuscular Disorders*, *22*, 199–207.

Shin, D. W., Pan, Z., Kim, E. K., Lee, J. M., Bhat, M. B., Parness, J., … Ma, J. (2003). A retrograde signal from calsequestrin for the regulation of store-operated Ca^{2+} entry in skeletal muscle. *Journal of Biological Chemistry*, *278*, 3286–3292.

Tomelleri, G., Palmucci, L., Tonin, P., Mongini, T., Marini, M., L'Erario, R., … Vattemi, G. (2006). SERCA1 and calsequestrin storage myopathy: A new surplus protein myopathy. *Brain*, *129*, 2085–2092.

Wang, S., Trumble, W. R., Liao, H., Wesson, C. R., Dunker, A. K., & Kang, C. H. (1998). Crystal structure of calsequestrin from rabbit skeletal muscle sarcoplasmic reticulum. *Nature Structural Biology*, *5*, 476–483

Wang, L., Zhang, L., Li, S., Zheng, Y., Yan, X., Chen, M., … Luo, D. (2015). Retrograde regulation of STIM1-Orai1 interaction and store-operated Ca^{2+} entry by calsequestrin. *Science Reports*, *5*, 11349.

Zhang, L., Wang, L., Li, S., Xue, J., & Luo, D. (2016). Calsequestrin-1 regulates store-operated Ca^{2+} entry by inhibiting STIM1 aggregation. *Cellular Physiology and Biochemistry*, *38*, 2183–2193.

Zhao, X., Min, C. K., Ko, J. K., Parness, J., Kim, D. H., Weisleder, N., & Ma, J. (2010). Increased store-operated Ca^{2+} entry in skeletal muscle with reduced calsequestrin-1 expression *Biophysical Journal*, *99*, 1556–1564.

SUPPORTING INFORMATION

Additional Supporting Information may be found online in the supporting information tab for this article.

How to cite this article: Barone V, Re VD, Gamberucci A, et al. Identification and characterization of three novel mutations in the *CASQ1* gene in four patients with tubular aggregate myopathy. *Human Mutation*. 2017;38:1761–1773. https://doi.org/10.1002/humu.23338